Journal of Molecular Liquids 362 (2022) 119708

Contents lists available at ScienceDirect

Journal of Molecular Liquids

journal homepage: www.elsevier.com/locate/molliq

Investigating disordered phases of C_2Cl_6 using an information theory approach

Andrés Henao [a,b,*], David Angulo-García [c], Gabriel J. Cuello [d], Philippe Negrier [e,f], Luis Carlos Pardo [g,*]

[a] Dynamics of Condensed Matter, Chair of Theoretical Chemistry, University of Paderborn, Warburger Str. 100, D-33098 Paderborn, Germany
[b] Nextmol (Bytelab Solutions SL), Carrer de Roc Boronat 117, 08018 Barcelona, Spain[1]
[c] Grupo de Modelado Computacional-Dinámica y Complejidad de Sistemas, Instituto de Matemáticas Aplicadas, Universidad de Cartagena, Carrera 6 36-100, Cartagena de Indias 130001, Colombia
[d] Institut Laue-Langevin, 71 avenue des Martyrs, 38042 Grenoble Cedex 9, France
[e] Université de Bordeaux, LOMA, UMR 5798, F-33400 Talence, France
[f] CNRS, LOMA, UMR5798, F-33400 Talence, France
[g] Grup de Caracterització de Materials, Departament de Física, EEBE, Universitat Politècnica de Catalunya, Avgda. Eduard Maristany 16, E-080197 Barcelona, Catalonia, Spain

ARTICLE INFO

Article history:
Received 3 February 2022
Revised 20 June 2022
Accepted 22 June 2022
Available online 30 June 2022

ABSTRACT

Many materials of interest and processes relevant to life are based in disordered phases. This disorder can be either positional, orientational or both as in the case of liquids. Unfortunately, the study of disordered phases is inherently difficult given the lack of periodicity as in ordered crystals. In this work we use neutron and X-ray diffraction experiments together with molecular dynamics simulations to study the local order and molecular movements in the disordered phases of hexachloroethane both in the liquid phase and in its plastic phase. The latter is a phase in which the molecular centres of mass form a long-range ordered crystalline lattice but molecules can rotate more or less freely. The concurrent use of diffraction experiments (Neutron and X-ray) and molecular dynamics simulations show that liquid structure mimics that of the disordered crystal at short distances. In order to extend the analysis to long distances, we have borrowed magnitudes from information theory that allow us to measure disorder and correlation. We also use the Kullback-Leibler divergence, an indicator of how similar two structures are to study the differences between plastic and liquid phases, as well as the structural difference at varying temperatures. We thus also offer in this work a common framework to characterize the structure of any disordered phase firmly based on probability and information theory. The advantage of our proposed methodology is that it can be used both to characterize the disorder and to perform comparisons of disordered materials with different degrees of freedom such as liquids and disordered crystals.

1. Introduction

Many biochemical processes of interest like protein folding or molecular recognition occur immersed in a disordered phase such as liquid water [1,2]. Furthermore, many materials of technological interest have an intrinsic disorder. Indeed, in some of the most promising new materials the centre of mass of the molecules form a crystalline phase being the molecules orientationally disordered, forming the so called Orientationally Disordered Crystals (ODIC) or plastic phases [3,4]. The utilization of disordered ODIC phases constitutes a new technology, still in development, that can be found in solid-state based cryogenic techniques [5,6]. Plastic phases are also an alternative to the dangerous and highly pollutant liquid-based electrolytes in lithium ion batteries [7].

Despite the importance of disordered phases, there is not a common frame to study the structure of those materials in any disordered phase such as the aforementioned liquids or ODICs. Indeed, many times the investigation of those structures, and the comparison between them, is not based on clear, quantitative foundations. In other words, questions such as "how similar two disordered structures are?" are usually answered in a vague and qualitative way or using low sensitive quantities such as the radial distribution function.

Hexachloroethane (C_2Cl_6) is a very interesting material because, due to its molecular symmetry, it shows a plastic phase in addition to the fully disordered liquid and the completely ordered crystalline phases. Fig. 1 shows a cartoon of the molecule. Liquid C_2Cl_6 is considered as a non-associated liquid because the steric effects are the most important to understand its structure, which

* Corresponding authors.
E-mail addresses: ahenaoa@unal.edu.co (A. Henao), luis.carlos.pardo@upc.edu (L. C. Pardo).
[1] Current address.

https://doi.org/10.1016/j.molliq.2022.119708
0167-7322/

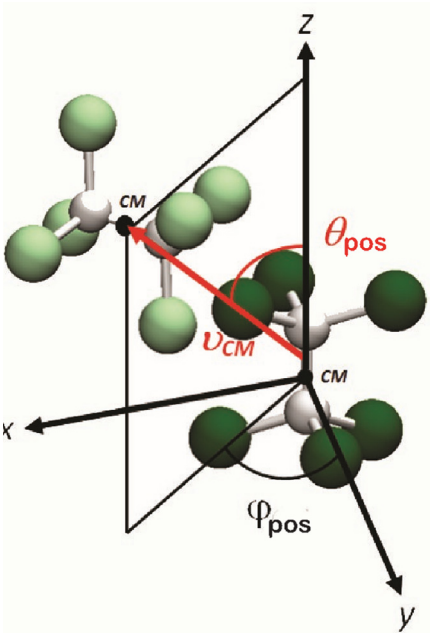

Fig. 1. Reference axis definition for the Euler angles study on the molecule C_2Cl_6. Angles θ_{pos} and φ_{pos} describe the position of any molecule relative to a reference molecule (with darker chlorides in the figure) using the vector $\sim v_{CM}$ that joins their centers of masses. Axis definition is the same as in our previous study on the liquid phase in order to ease comparison [20].

are well described by the van der Waals picture. Hexachloroethane presents three different solid phases [8,9]: orthorombic between 4 and 318 K, monoclinic [10] between 318 and 344 K and a plastic phase which is stable from 344 K up to the melting temperature T_m = 458 K [11]. This plastic phase has a body centered cubic unit cell (BCC). The positional disorder in the plastic phase comes from the fact that the space group is $Im\bar{3}m$ and a corresponding site group

m3m, but the molecule has a lower symmetry $\bar{3}m$. Therefore, the orientational disorder appears for the molecule to fulfill with the site group symmetry [12].

Regarding the structure of the plastic phase, in 1981 Gerlach et al. [12] conducted a neutron powder and single-crystal investigation and later Gerlach et al. [13] compared the previous results to a model structure of the plastic phase from a Monte Carlo (MC) method. In 1988 Gerlach and Prandl [14] studied the orientational ordering in the plastic phase using diffuse X-ray scattering and later (Gerlach et al. [15]) with elastic and quasielastic neutron scattering. Criado and Muñoz [8] performed Molecular Dynamics (MD) simulations on the plastic phase of C_2Cl_6 and they used their results to interpret inelastic neutron scattering experiments [9]. Negrier et al. also studied the symmetry of the plastic phase [10]. In this work we have improved the agreement with diffraction experiments with respect to that of Criado and Muñoz.

The intramolecular geometry of C_2Cl_6 has been previously investigated by means of electron diffraction in the gaseous and solid states [16,17]. In those works, the authors obtained bonds and angles that define the geometry of C_2Cl_6, but those parameters were not able to reproduce the structure of the molecule obtained from neutron diffraction experiments in the plastic phase. Later, using a Bayesian fit to the experiment the intramolecular geometry was determined [18]. This produced a better set of molecular parameters to use as an input for molecular dynamics (MD) simulations, in better agreement with the experimental plastic phase structure.

No experimental studies on the structure of liquid C_2Cl_6 have been performed (to our knowledge). Given its van der Waals symmetry (as explored by Slovokhotov et al. [19]) the boiling temperature is 1 K above the melting point at ambient pressure, producing the C_2Cl_6 sublimation and making any attempt to perform experiments unsuccessful. Therefore a simulation study is ideal to gain knowledge on the liquid and to obtain further comparisons to the plastic phase. We have already presented a molecular dynamics study on the structure of the liquid phase of C_2Cl_6 [20].

Information theory is a powerful approach for establishing a set of magnitudes to study and compare any disordered phase, even with different degrees of freedom. In this work we add to the magnitudes already introduced by some of us [21] the Kullback–Leibler divergence (KL divergence hereafter). This magnitude allows to investigate in a quantitative way differences between *N*-dimensional Probability Density Functions (PDFs), as those encoding the structure of disordered phases. KL divergence has been used before for other purposes, for instance to analyze similarities and change of conformations in protein ensembles [22] or to decipher fine structural properties of DNA [23]. Here we use it as a general measure that accounts for differences between the structure of disordered phases. This magnitude is to be added to the Shannon entropy (H) and mutual information (MI) quantities already defined in the context of disordered phases for the study of a single phase [21].

We will focus in this work on the study of the local structure and dynamics of the plastic phase, using both experiments and simulations. In addition we will use information theory in order to gain insights on its local ordering at short and long separation lengths between molecules, and we will perform a comparison with the liquid phase structure.

2. Methods

2.1. Experimental

A sample of C_2Cl_6 with a 99% purity was purchased from Sigma-Aldrich and used to perform the diffraction experiments without any further purification. The details of the neutron scattering experiments have been reported by us elsewhere [18].

2.1.1. X-ray diffraction

X-ray powder diffraction experiments were performed using a horizontally mounted INEL cylindrical positionsensitive detector (CPS120) equipped with a liquid nitrogen 600 series Cryostream cooler from Oxford Cryosystems with a temperature accuracy of 0.1 K. We have chosen a Debye–Scherrer geometry to perform the experiments. The detector is equipped with 4096 channels, providing an angular step of 0.029° (2θ) between 2° and 120°. Monochromatic Cu Kα_1 radiation (λ = 1.54056 Å) was used with an asymmetric focusing incident-beam curved quartz monochromator. The channel-angle conversion was calibrated by means of cubic spline fittings in order to correct the deviation from angular linearity in a position-sensitive detector using the cubic phase $Na_2Ca_3Al_2F_{14}$ mixed with silver behenate [24,25] as an external calibration standard. The samples were introduced into 0.3 mm-diameter Lindemann capillaries. Samples were rotated along their longitudinal axes during data collection to minimize the effects of preferred orientations. X-Ray patterns were obtained isothermally

between 346 K and 375 K. Acquisition times were at least 60 min, and a stabilization time of at least 5 min at each temperature before data acquisition was selected.

2.2. Simulation details

MD simulations were performed for the plastic and liquid phases of C_2Cl_6 on a 2000 molecules system. In the case of the BCC plastic phase, a supercell of 10 × 10 × 10 unit cells was used with the positions of the molecules corresponding to the BCC crystal and a random orientation for all the molecules. The simulation was performed at a temperature T = 400 K and a pressure P = 1 atm. In order to obtain the liquid phase, the final equilibrium configuration from the plastic crystal was used for a simulation at the thermodynamic conditions of the liquid [11], namely T = 458 K and P = 1 atm. Simulations were also performed on a small system of 504 molecules using the BCC lattice (6 × 6 × 7 unit cells) at 6 different temperatures (within the stability range of the BCC plastic phase) to obtain results on the lattice parameter expansion, T = 344, 360, 380, 400, 413, 423 K. For all the simulations, 1000 configurations were collected after reaching equilibrium and saved every 1 ps.

All the MD simulations were performed using the Gromacs 4.5 [26] package. The potential parameters were chosen from the Gromos53a6 [27] force field (6–12 Lennard Jones). Other general conditions were: Δt = 2 fs (during 500 ps), shifted cut-off from 16 to 17 Å for Lennard-Jones interactions and 20 Å for Coulomb pairs. The Particle Mesh Ewald (PME) was used beyond the electrostatic cut-off for the reciprocal space sum. The internal geometry of the molecule, i.e., the equilibrium bond distances and angles were taken from our previous study by fitting the long q-range of the structure factor [18]. Finally the analysis was made over the last uncorrelated 300 ps.

2.3. Euler angles and axes definition

A full determination of the molecular ordering can be achieved by studying the relative position and orientation of a given molecule with respect to a central one at a given distance. The three degrees of freedom related to the position of the centre of mass of a molecule are fully described by the distance between that point and the centre of mass of a reference molecule (d) and the bivariate distribution $p(\theta_{\text{pos}}, \varphi_{\text{pos}})$ at a selected distance d. The angles participating in the bivariate distribution θ_{pos}, φ_{pos} are depicted in Fig. 1 and correspond to the standard definition of spherical coordinates.

To define the orientational configuration of a molecule at a specific point, we use the Z − Y' − Z" proper Euler angles convention [28]. The trivariate distribution $p(\theta_{\text{ori}},\varphi_{\text{ori}},\psi_{\text{ori}})$ fully determines the probability of finding a molecule with a given orientation at a given position $d,\theta_{\text{pos}},\varphi_{\text{pos}}$ with respect to a central molecule (see Ref. [20] for a more detailed description).

We therefore can fully determine the structure of any disordered phase by the use of the six-dimensional probability distribution function $p(d,\theta_{\text{pos}},\varphi_{\text{pos}},\theta_{\text{ori}},\varphi_{\text{ori}},\psi_{\text{ori}})$. It must be pointed out that to correct for the effects of the projection of spherical coordinates, instead of calculating the PDF as a function of θ_{pos} and θ_{ori} it will be calculated as a function of their cosine, as it is usually done. It is also important to notice that, the description of solid phases, including plastic phases, is usually done from the laboratory reference system. In our case we are calculating the *relative* position of a pair of molecules separated by a given distance. This means that "position", in our case, is indeed a convolution of the orientation of the molecule with respect to the crystalline lattice with the vibrational movement of the molecules (both the reference one and the neighbour).

2.4. Information theory

2.4.1. Shannon entropy

We will use an information theory based framework to analyze the relative position and orientation between molecules to go beyond the usual analysis based on quantities such as the radial distribution function, or vector correlations. First of all we will use the Shannon-entropy that measures the disorder present in a given N-dimensional PDF, that might be related to molecular position, orientation, or a combination of any of the five angles describing molecular short range order. The Shannon-entropy is defined as:

$$H(x) = -\sum p(x)\log p(x) \tag{1}$$

being $p(x)$ the PDF related to an angle or any combination of them, i.e. can be related to 1-fold up to a 5-fold PDF in our case. In the case of a crystalline solid, Shannon-entropy is low since the PDF of any of the quantities related with position and orientation is structured (PDFs have clear and defined maxima and minima), and would be maximum for a structure-less flat, PDF. Therefore, in a liquid where the PDFs are less peaked, it will result in a higher value of Shannon-entropy (see [21] for an example on a toy-system). The Shannon-entropy of a convenient combination of all magnitudes determining molecular distribution (distance and angles determining position and orientation) can eventually be related to thermodynamic entropy (see our previous work [29]) via proper normalization. However we will use Shannon entropy in this work as a tool *per se* to investigate molecular ordering.

2.4.2. Mutual information (MI)

This quantity is a measure of correlation between variables. It can again be calculated from any PDF coming from a combination of angles (in two or more dimensions). However, in this work we will use it only to characterize correlations between the positional angles θ_{pos} and φ_{pos}, and it is thus defined as:

$$I(\theta_{pos},\phi_{pos}) = p(\theta_{pos},\phi_{pos})\log\frac{p(\theta_{pos},\phi_{pos})}{p(\theta_{pos})p(\phi_{pos})} \tag{2}$$

2.4.3. Kullback-Leibler divergence

Finally we will use the Kullback-Leibler divergence to measure how "close" the liquid structure is to that of the BCC phase:

$$D_{KL} = \sum_{\{x_i\}} p\{x_i\}\log\frac{p\{x_i\}}{q\{x_i\}} \tag{3}$$

where $p\{x_i\}$ and $q\{x_i\}$ are the PDFs associated to any one of the disordered phases. In this work $\{x_i\}$ = $(\cos(\theta_{\text{pos}}),\varphi_{\text{pos}})$ is a compact way to write that the summation is to be taken pixel by pixel for the whole 2D-PDF related to positional variables of the two phases. D_{KL} is not, in general, symmetric and hence we use its symmetrized version: the average of $D_{\text{KL}}(p,q)$ and $D_{\text{KL}}(q, p)$. For that reason $p\{x_i\}$ and $q\{x_i\}$ can be associated to any of the two disordered phases. We have, therefore a way to *unambiguously* determine how close two structures are, given that both PDFs must be normalized to unity.

3. Results

3.1. Neutron and X-ray diffraction on the plastic phase of hexachloroethane

In this section, we will focus on the comparison of MD simulations with X-ray and neutron diffraction experiments. First, we have calculated the experimental lattice parameter as a function

of the temperature coming from X-ray diffraction, within the stability range of the plastic BCC phase of C_2Cl_6 (344–457 K), and we have compared it with the equilibrium configurations of the simulation in a NPT ensemble. The lattice parameter temperature dependence is compared to previous powder neutron diffraction data reported by Gerlach et al. [12] and a previous simulation of Criado and Muñoz [8] (see Fig. 3). Our MD results agree with the experimental data, and fit better than the results of Criado and Muñoz [8]. This shows that the force field and intramolecular structure used in this work reproduces better the density and thermal expansion of the crystal lattice than that of previous works. This can be ascribed to (i) a set of refined intramolecular parameters from our previous work [18] and (ii) a different shape of the potential (we used a 6–12 Lennard Jones instead of the Buckingham potential used by Criado and Muñoz).

3.2. Static structure factor

In order to compare the experimental structure factor with that coming from MD simulation we compute the experimental static structure factor $S_{exp}(q)$ as the Fourier transform of the total pair distribution function $g_{total}(r)$, properly weighted by the contribution of the neutron coherent scattering lengths of the atoms (b_C = 0.646 fm and b_{Cl} = 0.9577 fm), namely:

$$S_{exp}(q) - 1 = \frac{4\pi\rho}{q}\int_0^{r_c} r[g_{total}(r) - 1]\sin(qr)dr \quad (4)$$

We set ρ = 1, as it acts as a scaling factor when comparing with the experimental results, r_c is the cut-off of the integration. The cut-off value is chosen large enough such that $g_{total}(r_c) - 1 \approx 0$, and to minimize the derivative of $g'_{total}(r_c)$, so that the pair distribution function is as flat as possible. This allows us to avoid spurious effects at low q-values when Fourier transforming the total pair distribution function.

The experimental static structure factor $S_{exp}(q)$ obtained from neutron diffraction can be seen in Fig. 4 together with the results obtained from molecular dynamics simulation $S_{MD}(q)$ using Eq. (4). As it can be seen, the static structure factor obtained from the simulation does not fit experimental data since in the last case there is a broadening coming from the instrument's resolution.

The instrumental resolution function $R(q)$ is described as a Gaussian function with a FWHM determined by the q-resolution function [31]. This means that $R(q)$ corresponds to a set of Gaussian functions at each q-point (see the inset in Fig. 2 where two Gaussian functions defined for two different values of q are shown).

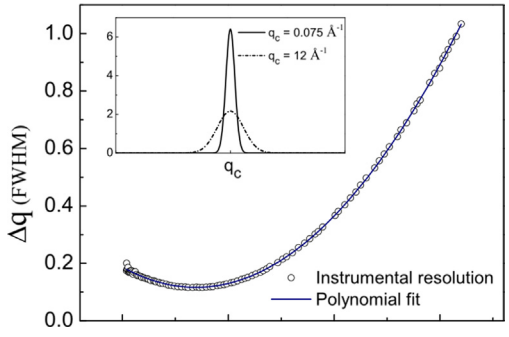

Fig. 2. Instrumental resolution function Δq as a function of q from the D4c3 [30] diffractometer. Hollow circles are the experimental values from the calibration sample and the thick line shows the polynomial fit (Eq. (5)). The inset shows two Gaussian functions with a FWHM determined by the value of Δq at a given q (q_c), at high q values the Gaussian function becomes wider.

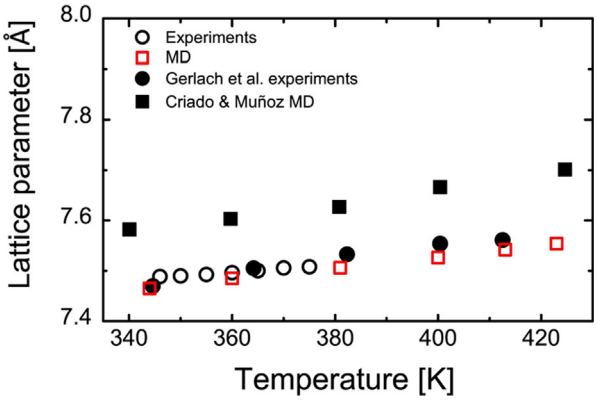

Fig. 3. The lattice parameter as a function of the temperature within the plastic phase. Circles show experimental data, open symbols with our X-ray results and filled symbols for Gerlach et al. [12]. Squares show molecular dynamics (MD) simulations, open symbols show our results and filled symbols those of Criado & Muñoz [8].

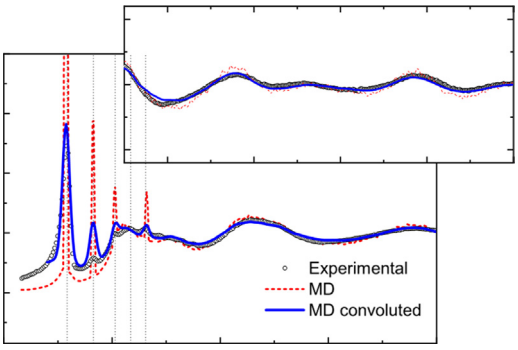

Fig. 4. Static structure factor of C_2Cl_6 at T = 400 K. Hollow circles: experimental data $S_{exp}(q)$. Dashed line: structure factor directly obtained from MD trajectories $S_{MD}(q)$ and after convolution with the experimental resolution $S_{MDc}(q)$.

Fig. 2 shows the q-resolution (Δq) as a function of q obtained for a calibration sample. We performed a quadratic fit to this function which is given by the following expression ($\Delta(q)$ in Å):

$$\Delta(q) = 0.00584q^2 - 0.04057q + 0.18696 \quad (5)$$

In order to obtain the function $S_{MDc}(q)$ to be compared with the experiment, we must compute the convolution of $S_{MD}(q)$ with $R(q)$, i.e, with a Gaussian function centered at q with standard deviation given by the relationship $FWHM \approx 2.3548\ \sigma$:

$$S_{MDc}(q) = \sum_i^{N_p} S_{MD}(q_i)R(q_i - q) \quad (6)$$

$$S_{MDc} = \sum_i^{N_p} S_{MD}(q_i)\frac{2.3548}{2FWHM}\exp\left[-\frac{1}{2}\left(\frac{2.3548(q_i - q)}{FWHM}\right)^2\right] \quad (7)$$

In Eqs. (6) and (7), $S_{MD}(q_i)$ is the original MD static structure factor and q_i runs for every point in $R(q_i)$, which in our case correspond to the interval $q_i \in [0.075\ Å^{-1}, 14\ Å^{-1}]$ in steps of 0.025 $Å^{-1}$, the value of $FWHM$ is given by $\Delta(q)$, and N_p is the number of experimental points. We can thus rewrite:

$$S_{MDc}(q) = \sum_i^{N_p} S_{MD}(q_i)\frac{2.3548}{2\Delta(q)}\exp\left[-\frac{1}{2}\left(\frac{2.3548(q_i - q)}{\Delta(q)}\right)^2\right] \quad (8)$$

As we have already stated, the function $S_{MD}(q)$ is more peaked than the experimental counterpart $S_{exp}(q)$. In experiments, the broadening of the diffraction peaks comes from two sources: the first one is due to the intrinsic disorder of the plastic phase (orientational disorder and thermal agitation). The second factor is related to the limited instrumental resolution. The MD simulation intrinsically considers the first factor, but the second one is not present in simulations and must be included.

In Fig. 4 we show $S_{MDc}(q)$, the calculated convolution of $S_{MD}(q)$ with the instrumental resolution function $R(q)$. The result of that convolution corresponds to the thick line in Fig. 4. Including the resolution function in the $S_{MD}(q)$ allows the agreement with the experiment. This result thus shows that the instrumental resolution function should be included in the calculation of the MD static structure factor. The agreement, although good, is not perfect. The reason for that can be related to some preferential orientation of the sample crystallization: this would explain the almost perfect agreement for the first diffraction peak, in comparison with the second one.

Fig. 4 shows $S_{exp}(q)$ and S_{MDc} up to a value of $q = 8$ Å^{-1}. For larger values of momentum transfer, the contribution of intermolecular ordering is small compared to the contributions from the geometry of the molecule. Although there is no way to completely separate the intramolecular contributions, the main contribution in the small q range comes from intermolecular distances [32]. This can clearly be seen in the $S_{MD}(q)$, where the well defined peaks correspond to the positional ordering of the BCC phase. In order to support this statement, we have computed the position of Bragg peaks within the q-range of the experiment using the equilibrium lattice parameter from MD, i.e. 7.54 Å. These peaks are shown as vertical dotted lines and, as it can be seen, they perfectly match with the MD peaks. We also show in the inset the excellent agreement between the experiment and the MD simulations. This agreement, however, should be taken cautiously since, as previously explained, the structure of our molecular model is indeed taken as a fit to this high momentum transfer region [18].

3.3. Dynamics in the liquid and plastic phases

We have computed the mean-square displacement (MSD) for the liquid and BCC plastic phases at $T = 400$ K (see Fig. 5). In this figure it is possible to see a positional motion for the plastic phase (thick line) at short times that is related to thermal motion. For longer times (greater than 20 ps) there is no motion of the molecular centers of mass. On the countrary, for the liquid phase (dotted line) we obtain the typical MSD behavior for long range molecular diffusion (for further details see [20]).

In order to characterize the relaxation properties of molecules in the liquid and plastic phases, we compute the reorientational correlation function (RCF). Orientationally disordered phases have an RCF that decays to zero, while for a fully ordered crystal the orientations are fully correlated, with a value close to 1 at all times. RCF can be obtained as:

$$RCF_l = \langle P_l\left[\vec{U}_\alpha(0) \cdot \vec{U}_\alpha(t)\right]\rangle \quad (9)$$

where P_l is the first (P_1) or second (P_2) rank Legendre polynomial:

$$P_1(x) = x \quad (10)$$

$$P_2(x) = \frac{1}{2}(3x^2 - 1) \quad (11)$$

and $\vec{U}_\alpha$ is the unit vector which points along a given α axis in the C_2Cl_6 molecule. We did the calculations for two different α vectors, namely the C-C and the C-Cl vectors. Fig. 6 shows the first Legendre

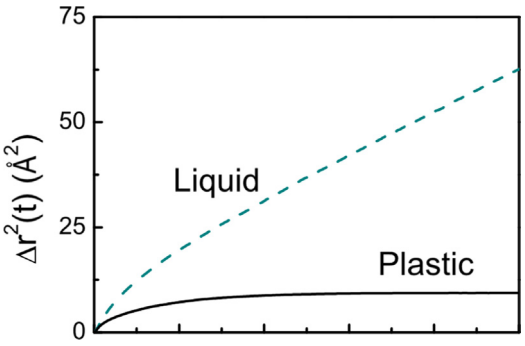

Fig. 5. Mean-square displacement for the plastic (thick line) and liquid (dashed line) phases. For the plastic (liquid) phase a temperature of $T = 400$ K, ($T = 458$ K) was used. (For further details see [20]).

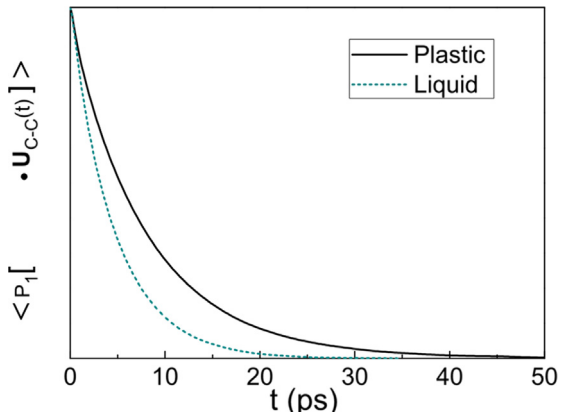

Fig. 6. Reorientational correlation function for the C-C vector: plastic (thick line) and liquid (dashed line) temperatures.

polynomial of the C-C vector for the liquid and plastic phases. They both decay to zero, clearly showing the orientational disorder present in the plastic phase. As expected, the decay is faster in the liquid phase. Results for the C-Cl vector and second Legendre polynomial follow the same trends and are not shown.

We computed the reorientational times obtained from the integral of the RCF. The ratio between the reorientation times τ_1 and τ_2 gives information about the kind of reorientation of the molecules. For a rotation of molecules that is more diffusive, i.e. consisting of small angular jumps [33,34], the reorientation times decay exponentially with a time constant $\tau_l = [D_R l(l+1)]^{-1}$, which corresponds to a ratio $\tau_1/\tau_2 = 3$. Here, D_R is the rotational diffusion coefficient and can be measured experimentally. For rotations that consist of larger jumps, the ratio τ_1/τ_2 is expected to be smaller.

It was found for the plastic phase: $\tau_1/\tau_2 = 2.55$ for the CC vector and $\tau_1/\tau_2 = 2.28$ for the C-Cl vector. In the liquid phase: $\tau_1/\tau_2 = 2.56$ for the C-C vector and $\tau_1/\tau_2 = 2.58$ for the C-Cl vector. These results suggest that reorientation is performed in both cases via jumps. Moreover, for the plastic phase the values of τ_1/τ_2 for both C-C and C-Cl vectors are slightly different, being very similar in the case of the liquid phase. This seems to point out to the fact that reorientations occur more isotropically in the liquid phase than in the plastic phase.

3.4. Short range order in the liquid and plastic phases

In order to compare the short range order of liquid and plastic phases at the shortest distances, the same analysis done for the liquid phase of C_2Cl_6 in our previous work [20] was done for the first

eight neighbors in the BCC plastic phase. In the upper panel of Fig. 7 we show the position of these first neighbors for both phases with respect to a central molecule, as a PDF of the angles φ_{pos} and $\cos(\theta_{pos})$ depicted in Fig. 1.

In a plastic phase the centers of mass of the molecules are forming a fixed crystalline structure. What is the meaning of $p(\varphi_{pos},\cos(\theta_{pos}))$ considering that it is related to the position of a neighboring molecule with respect to a central one, being their centres of mass fixed? The answer is that the central molecule rotates with respect to the fixed reference frame given by the crystalline lattice, *and so does the axis attached to it*. Therefore the PDF in the case of the BCC phase is indeed related to the rotations of the central molecule with respect to the crystalline lattice, determined by the center of mass of the neighboring molecules (recall that φ_{pos} and θ_{pos} angles are related to a vector pointing to the centre of mass of a neighbor).

The eight nearest neighbors in the BCC phase are molecules located in the vertices of the cubic lattice. The representation of the BCC lattice is shown as an inset in the middle of Fig. 7. In the BCC phase, the reference molecule is oriented in the [1 1 1] diagonal as depicted in Fig. 7. This relative orientation with respect to the crystalline lattice can be seen in the positional map, that shows two elongated spots in ($\cos(\theta_{pos}) = \pm 1$) in Fig. 7 associated to the molecules parallel to the C-C direction. The remaining six vertices are occupied by molecules that appear as clear spots at locations ($\cos(\theta_{pos}) = \pm 0.4$).

Relative molecular orientation *at a given position* ($\varphi_{pos},\theta_{pos}$) is completely defined by the trivariate distribution $p(\varphi_{ori},\psi_{ori},\theta_{ori})$. However, visualization of the 3-D PDF is a difficult task, and for this reason we show in the bottom panels of Fig. 7 the two 2-D projections using as the common *x* axis $\cos(\theta_{ori})$.

Due to the lattice symmetry, it is sufficient to study one of the positional spots in the ($\varphi_{pos},\cos(\theta_{pos})$) maps associated with a neighboring molecule located at a given BCC vertex with respect to the central molecule. However, for consistency we have studied the relative molecular orientations for two molecules: one located in the direction parallel to the C-C molecular axis ([1 1 1] direction in the figure) in the bottom left panel, and one located in the [11–1] direction (approximately perpendicular to the C-C axis) in the bottom right panel.

The PDF $p(\cos(\theta_{ori}),\varphi_{ori})$ in Fig. 7 shows that two neighbor molecules avoid having the C-C axis parallel: there are no elongated spots for $\cos(\theta_{pos}) = \pm 1$. In other words they avoid having contact through chlorine atoms. These results are consistent with those previously reported for the BCC structure [8].

Moreover the map of $p(\cos(\theta_{ori}),\psi_{ori})$ shows six spots located every 60°. This agrees with successive dihedral angles between chloride atoms attached to each carbon atom. The molecules are thus performing an uniaxial rotation along the C-C atom, in addition to the overall rotation.

We compare now the results for BCC phase with that of the liquid phase. The results on top panels clearly show that the position of one molecule, given a central one, is astonishingly similar for both phases. The positions of the plastic phase are better defined as expected, and they correspond to the unit cell. This result agrees with the characterization of the dynamics: there is not a continuum of possible relative positions. In other words, rotations must occur when transitioning from a high-probability spot to another one, thus implying a jump across a potential energy barrier. This means that rotations are performed via jumps. Moreover, in the probability map of the BCC phase, spots are separated and well defined, but in the liquid phase these are closer and bigger. This

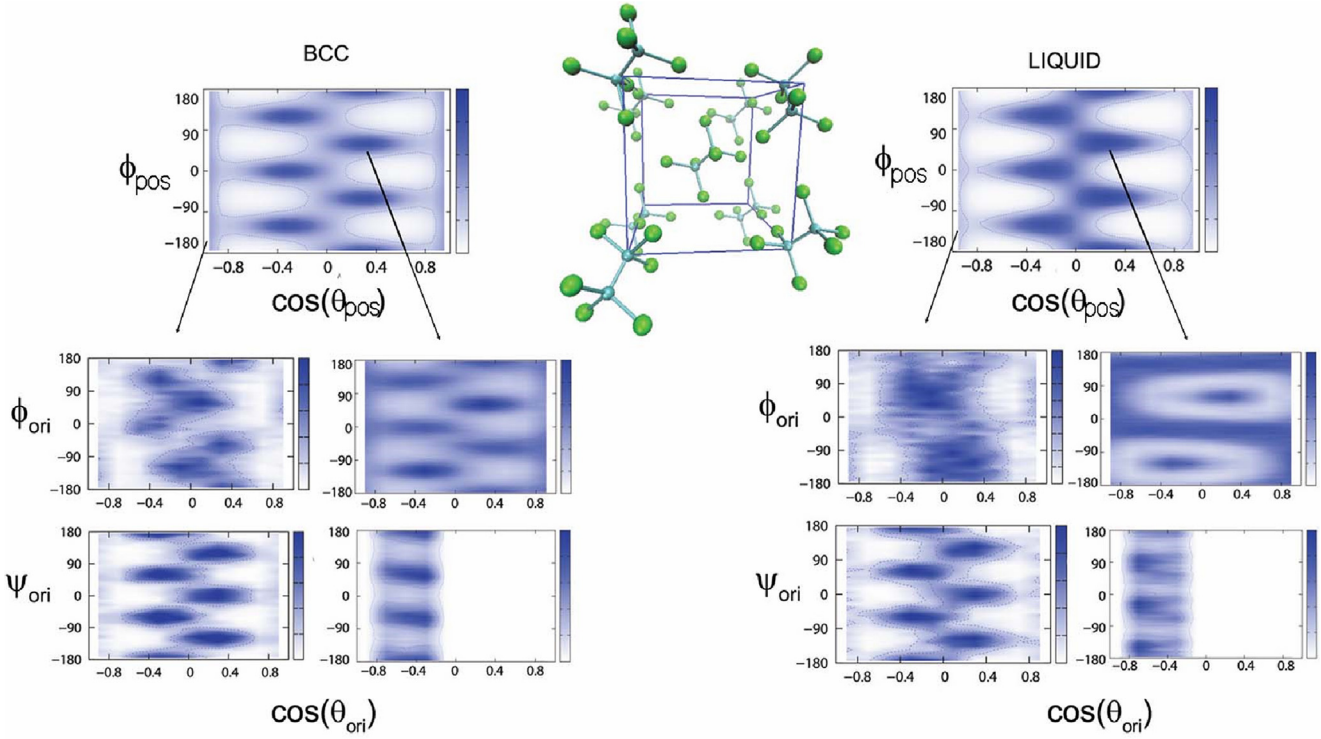

Fig. 7. First neighbor analysis for the plastic BCC phase (left) and the study previously done by the authors on the liquid phase [20] (right) of C_2Cl_6. At the top, the positional bivariate maps $p(\cos(\theta_{pos}),\varphi_{pos})$. In the middle, the orientational $p(\cos(\theta_{ori}),\varphi_{ori})$ maps. At the bottom, the orientational $p(\cos(\theta_{ori}),\psi_{ori})$ maps. The arrows show the regions that are analyzed: one of the equatorial positions and one of the polars, as it was studied for the liquid in the last section. The inset of the figure in the center shows the corresponding BCC unit cell, with some of the possible orientations.

causes that jumps are more isotropic in the liquid phase, also in agreement with our results concerning the dynamics of both phases.

An unexpected result is that also the relative orientational order between two molecules is similar in both phases. The difference lies in the fact that molecules in the liquid can continuously move between some of the orientations, while in the plastic phase there are only some allowed orientations. Specifically, in both phases the contact between chlorine atoms is avoided (see $p(\cos(\theta_{ori}),\varphi_{ori})$), and in both phases molecules perform fast uniaxial rotations (see $p(\cos(\theta ori),\psi ori)$).

3.5. Information theory based analysis

Characterization and comparison between the molecular ordering *at a given distance* of disordered phases can be performed at a high level of specificity determining the projections of the 5-dimensional PDF containing all positional and orientational angles defining the molecular relative arrangement as done in the last section. However this high level of specificity has two main drawbacks: Firstly, in practical terms, it cannot be routinely performed for all distances, and secondly it does not give a measurement on how ordered are molecules or how different the molecular arrangements are at a given distance between two different phases. Therefore we aim to analyze the long range order (neighbors for all coordination shells) using the information theory tools introduced in a previous section.

We will focus in the relative positional ordering, therefore, we will only analyze the positional order encoded in $p(\cos(\theta_{pos}),\varphi_{pos})$. Instead of performing the analysis as a function of the distance we will order the molecules for both the liquid and the plastic phase by their distance to a reference molecule, i.e. we will calculate the molecular coordination number (MCN) denoted by N, and will extend the analysis up to neighbor number 75. The use of MCN instead of the distance is made to highlight the presence of different coordination shells. The results are depicted in Fig. 8.

Pair distribution function. In Fig. 8 we show the pair distribution function $g_{CM-CM}(r)$ (top panel) of molecular centres of mass as a function of MCN. This is done for both the liquid and the BCC phases.

It is important to note that the radial pair distribution function encodes the information of local density around a central molecule. It does not contain any information about relative orientations or positions of molecules, i.e., a maximum in $g_{CM-CM}(r)$ cannot be associated *a priori* to any given molecular configuration. One of the needs for the information theory-based analysis is indeed to investigate if features in $g_{CM-CM}(r)$ can be associated to any special molecular ordering.

In the case of the BCC plastic phase (red line), $g_{CM-CM}(r)$ shows well defined shells. It is very interesting to note, however, that not all the shells of the BCC phase are limited by a pair distribution function going to zero as it would be the case for a perfect crystal. The first two neighboring shells appear at 8 and 14 molecules, and correspond to the nearest and nextnearest neighbors in the BCC lattice: in this case the second shell is seen as a shoulder of the first $g_{CM-CM}(r)$ peak.

In the case of the liquid (blue line), the pair distribution function shows less structure than its BCC counterpart and its features are damped at much shorter distances than that of the plastic phase, as expected. However, it should be pointed out that the first broad peak of the liquid together with the associated shoulder has a minimum at $N = 14$, and therefore it mimics the same shell definition (at short distances) as in the BCC phase.

1. *Shannon Entropy H.*

The second panel of Fig. 8 shows the normalized Shannon entropy (H/H_∞) associated to the positional maps (variables cos (θ_{pos}) and φ_{pos}) for the two phases under study. Here H_∞ is the maximum value of the entropy that is obtained when N tends to infinity for each phase. Recall that H is maximum for a flat PDF with no information (a completely disordered structure in our case) and zero for a PDF with maximum information: a PDF with only one pixel (or voxel) with probability $P = 1$ [21].

For the case of the BCC phase the features in the pair distribution function correspond to changes in the normalized Shannon entropy H/H_∞. However it is remarkable that the trend of H/H_∞ is different depending on the behaviour of $g_{CM-CM}(r)$. When the pair distribution function reaches zero, i.e. well defined shells, H/H_∞ has a deep and clear minimum. When $g_{CM-CM}(r)$ does not reach zero (or even it is seen as a shoulder as for first and second shells), the changes in H/H_∞ are smooth. This suggests that not all shells play the same role in the BCC structure.

In the case of the liquid phase it is remarkable that we find low values of normalized Shannon-entropy for the very first neighbors that are of the same order of magnitude than those of the plastic phase. However, normalized Shannon entropy increases rapidly to reach values close to one after the first coordination shell. As expected, this function is much less structured for the liquid phase than for the plastic phase.

2. *Mutual information I_2.*

We depict the mutual information I_2 (see Eq. (2)), which measures the correlation between the positional angles θ_{pos} and φ_{pos} in each phase in Fig. 8. I_2 can take values between 1 and 0, which correspond, respectively to a case of full correlation between

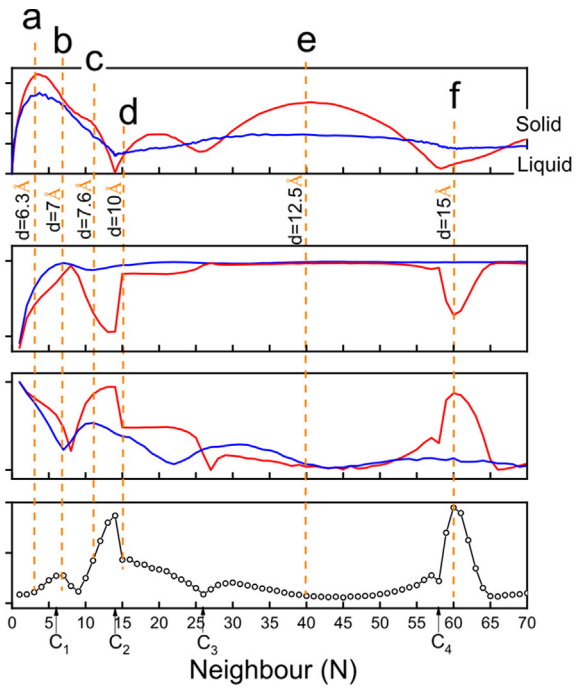

Fig. 8. Information theory analyses to compare the positional maps $p(\cos(\theta_{pos}),\varphi_{pos})$ between the BCC (red thick line) and liquid (blue line) phases. From top to bottom: Pair distribution function (g_{CM-CM}), the rescaled entropy (H/H_∞), the mutual information (I_2) and the Kullback-Leibler divergence. All quantities are represented as a function of the mean coordination number (MCN). We have added in the x axis arrows showing the limiting distances for successive coordination shells C_i. (For interpretation of the references to color in this figure legend, the reader is referred to the web version of this article.)

angles and no correlation at all. It shall be noticed that I_2 is negatively correlated in our case to the normalized Shannon entropy (see Fig. 8): Low values of H/H_∞ indicate higher order, meaning a higher correlation between the positional variables. Also, the value I_2 is more structured for the positional order in the liquid compared to H/H_∞ being more sensitive to structural changes.

The correlation between Shannon-entropy and mutual information can be explained if we write the expression relating the two quantities:

$$I(\theta_{pos};\phi_{pos}) = H(\theta_{pos}) + H(\phi_{pos}) - H(\theta_{pos};\phi_{pos}) \quad (12)$$

This means that if the 1D projection of the maps $\cos(\theta_{\text{pos}})$, φ_{pos} -i.e the marginal probability densities $p(\cos(\theta_{\text{pos}}))$ and $p(\varphi_{\text{pos}})$- in each axis gives as a result a non-defined PDF, mutual information will be mainly driven by the entropy associated to the 2D bivariate PDF: it would be a sort of normalized Shannon Entropy. As it can be seen in Fig. 8 this is exactly what is happening: $H(\theta_{\text{pos}})$ and $H(\varphi_{\text{pos}})$ are more or less constant, and the Shannon entropy associated to the bivariate positional maps leads the trend in the mutual information.

3.5.1. Comparison of positional maps at different distances

At this point it is interesting to analyse some positional maps at different coordination numbers, indicated by the vertical lines in Fig. 8 and the relation of these with the information theory measures. These maps are depicted for both the plastic and liquid phase in Fig. 9. As it was stated previously, Mutual Information follows an inverse trend with respect to the Shannon entropy, therefore we will focus the discussion on the Shannon Entropy only. It is important to recall that these maps *cannot be obtained from the lattice structure*: they do not represent the molecular position seen from the laboratory frame but from the molecular moving reference system (as stated in the methods section)

BCC phase:

- Point *a*, N = 3. Molecules are located, when seen from a central one, around the equatorial plane and in the poles as shown in section 3.4 (map *a* of Fig. 9). Since H/H_∞ increases up to point *b* this particular configuration is less defined as distance increases.
- Point *b*, N = 7. Molecules are still located as in point *a*, but, as it could be predicted by Shannon Entropy, the map is less defined (map *b* of Fig. 9).
- Point *c*, N = 11. As it can be seen when compared to the map in point *a*, there is a change in the structure: molecules occupy the "holes" left by the molecules by the first eight neighbours, i.e. maxima in positional bivariate maps for point *b* are in the places where we can find minima in point *a*. It is interesting to note that this change in structure has been captured by a sudden change in H/H_∞. It is also interesting that, contrary to the intuition, this particular arrangement is more defined as the distance increases, i.e. maps are more defined (not shown).
- Point *d*, N = 15. A sudden change takes place for H/H_∞ at N = 14. This is explained by the extreme change in the structure as seen in the map marked as *d* in Fig. 9.
- Point *e*, N = 40. Again a change in H/H_∞ indicates a change in the relative orientation of two molecules associated to a change in $g_{\text{CM}-\text{CM}}(r)$: at distances associated to the fourth peak, molecules repeat the same trend as in point *c*: they occupy the "holes" left by the neighbours in the previous shell *d*.
- Point *f*, N = 60. An extreme and unexpected decrease in Shannon entropy occurs at this distance, signalling an important ordering of the molecules. Looking at the map at point *f* we discover that this drop is associated with an also unexpected clear molecular arrangement: molecules at this distance tend to locate (with respect to a central molecule) as in shell *c*.

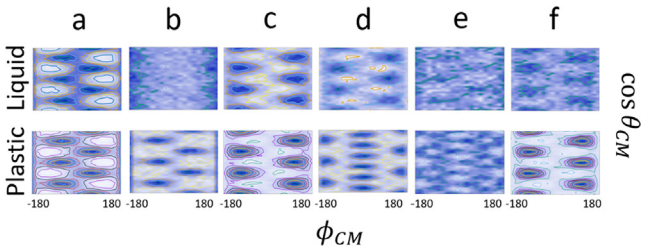

Fig. 9. Bivariate probability distribution function describing the relative position of moleclues for the distance market in Fig. 8.

Liquid phase:

- Point *a*, N = 3. Molecules are located as in the BCC phase: approximately in the equatorial plane and in the poles as stated in section 3.4. We also see an increase of H/H_∞, just like in the BCC phase, but the maximum of H/H_∞ is not as clear as in the plastic phase.
- Point *b*, N = 7. Contrary to what happens in the BCC phase, molecular configurations (as seen in the map b of Fig. 9) seem not to have a special ordering. It seems a transition state to the next molecular configuration. This lack of sudden molecular arrangement has been perfectly captured by the Shannon entropy.
- Point *c*, N = 11. Again for point *c* molecules seem to be in a specific configuration, and this configuration mimics that of the BCC phase.
- Point *d*, N = 15. The sudden change described in the BCC phase is no present in the liquid structure, as seen in the map of point *d*. This fact has already being captured by the lack of features in H/H_∞ in this distance region. Indeed, this point is a good example of the usefulness of distance-dependent Shannon Entropy calculations, namely, without analysing the circa of 70 2D maps describing the relative molecular positions of both phases, we know from H/H_∞ that a feature happening in the BCC phase is not happening in the liquid phase.
- Points *e* and *f*, N = 40, 60. The relative position of molecules is not well defined for very long MCNs such as 40 or 60, as it can be seen both in the maps and the Shannon entropy. However, it is astonishing that for point *f* positional ordering slightly resembles that of BCC phase: spots, although much less defined, are located at the same points as in the BCC phase.

3. *Kullback-Leibler divergence.*

Now that we have a clear picture of the location of molecules at different characteristic distances both in the BCC and liquid phases, we will compare both sutructures using the KL divergence as a function of MCN. KL diveregence is shown in the bottom panel of Fig. 8. According to the definition of KL divergence a low value indicates a high similarity: a low "distance" between the structures. The comparison of BCC and liquid phases guided by the results of KL-divergence has been divided in two regions. A first region from N = 1 to N = 14 (point *a* to point *d* in Fig. 9) where the Shannon entropy of the liquid phase has noticeable changes in its trend, and a second region for MCNs larger than N = 14, where liquid Shannon entropy is flat. In this second case, when calculating the KL divergence, the liquid phase will act simply as a disordered reference state, given that its entropy is maximum at this distance range and shows no marked features.

- Region *a*-*d*. As we can see in Fig. 9 the relative molecular position is very similar for points *a* and *c* while in point *b* the ordering in both phases is different. This feature is perfectly captured

by the KL divergence in Fig. 8: it has a local maximum at point *b*. After a small decrease, the dissimilarity between the two phases increases again due to the decrease in Shannon entropy of the BCC phase compared with the liquid phase. For larger distances it is interesting to note from Fig. 9 that no change in liquid structure is observed (this is reflected in a rather constant Shannon entropy) while the BCC phase suffers an extreme change when going from N = 14 to N = 15. This is clearly reflected in the KL divergence where there is a maximum when the BCC phase reorders in a new configuration while the liquid remains unchanged.

- Region *d-f*. As mentioned before, the Shannon entropy of the liquid phase has no special features (remains almost constant). Therefore the results of the KL divergence reflect the changes in the BCC phase where we have seen a further ordering at point *f* and thus presenting a new maxima at N = 60.

Temperature-dependent KL-divergence. KL divergence can also be used to determine differences of the molecular ordering of the same phase at different temperatures. In particular we have calculated the KL divergence in order to understand which part of the *relative* molecular configuration changes the most -either position or orientation- when varying temperature. In other words, when varying the temperature, which KL divergence will be greater? The one related to positional or the one related to orientational maps? We would like to stress that by relative position we mean relative position of two molecules at a given distance range. That means that lattice expansion will have no direct effect on the calculation since we have chosen the distance range defined by the first eight neighbours for all temperatures.

Fig. 10 shows the KL divergence between the maps encoding the relative molecular position $p(\theta_{\text{pos}},\varphi_{\text{pos}})$ and the relative molecular orientation ($p(\theta_{\text{ori}},\varphi_{\text{ori}})$ and $p(\theta_{\text{ori}},\psi_{\text{ori}})$), taking the map at 340 K as the reference system. As expected, relative position and orientation shows an increase in the KL divergence when increasing temperature. However the curve associated to the relative position increases more than that associated to relative orientation. It must be recalled, that the overall molecular tumbling is associated to the relative molecular position. Considering that an increase in temperature does not change the structure of the plastic phase, we can relate our result to a facilitation of the changes in the molecular jumps to reach different molecular orientations with respect to the lattice reference system.

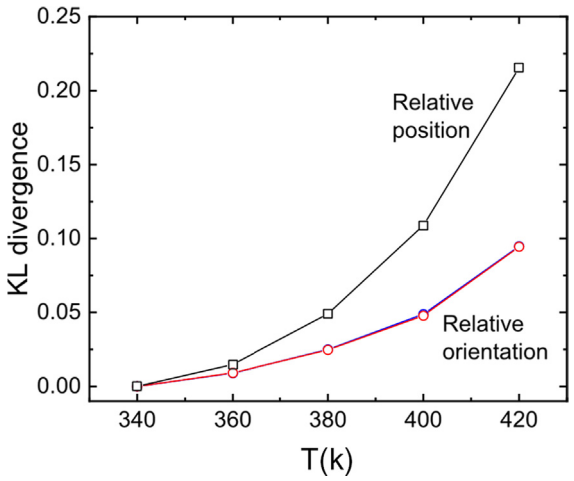

Fig. 10. Kullback-Leibler divergence as a function of temperature for the BCC phase taking the lowest temperature (340 K) as a reference state. We plot in the figure the results for the bivariate graphics of Fig. 7 at different temperatures describing both relative orientation and position of molecules.

4. Summary and conclusions

The structure of the C_2Cl_6 BCC plastic phase has been studied at a high level of detail for the first neighbors by comparing positional and orientational PDFs. In order to compare the positional ordering with that of the liquid phase as a function of the distance between two molecules, quantities borrowed from Information Theory have been used. This has been done using a new Force Field for C_2Cl_6 that has been successfully validated via comparison with X-Ray and Neutron diffraction patterns.

First of all the detailed analysis on the closest molecules in the first shell showed a positional and orientational ordering surprisingly similar between the plastic crystal with BCC symmetry and the liquid phase. This can be explained by the fact that for this molecule steric effects are the most important ones when determining molecular ordering. Therefore the molecular arrangement in both phases try to have a close packing avoiding the molecules to face chloride shells.

These results concerning the structure go along with our investigation of molecular rotation: it is not performed in a continuous way, molecules must perform jumps between energy barriers. Moreover, also in agreement with the structure investigation, molecules move more isotropically in the liquid than in the plastic phase.

Information theory is a valuable and important tool to analyze the results obtained with the study of distance-dependent molecular ordering. It did not only allowed to analyze a large data-set, that would have been time-consuming otherwise, but also provided quantitative results that complete the qualitative information provided by the detailed Euler angles analysis.

When analyzing the positional maps under the light of information theory, the mutual information showed more marked features related to the structure than the Shannon entropy. We introduce in this work the KL divergence that helped us to compare both structures: instead a monotonous increase of the KL divergence between both structures, we found marked features as a function of the distance.

The calculation of the positional maps describing relative molecular position have aided us to clearly show that the trends in molecular ordering are successfully captured by our information theory based analysis. This opens the door to simplify tedious analysis since it restricts the length regions that are worth to be studied.

Declaration of Competing Interest

The authors declare that they have no known competing financial interests or personal relationships that could have appeared to influence the work reported in this paper.

Acknowledgments

A. H. would like to acknowledge the funding by the FPUUPC grant from Universitat Politècnica de Catalunya and partial support provided by “Departamento Adminsitrativo de Ciencia Tecnologia e Innovacion - Colciencias” from Colombia through the program “Doctorados en el exterior – 2014”. L. C. P. acknowledges financial support from the Spanish AEI/MCIN through project PID2020-112975GB-I00 and the Catalan Government (Grant 2017SGR-42). D.A-G was financially supported by Minciencias and the Sistema General de Regalias SGR through Project BPIN 20200001003467. Autors A. H. and L. C. P. would like to acknowledge inspirational conversations with M. Periné.

References

[1] N. Steinke, R.J. Gillams, L.C. Pardo, C.D. Lorenz, S.E. McLain, Atomic scale insights into urea–peptide interactions in solution, Phys. Chem. Chem. Phys. 18 (2016) 3862–3870.

[2] Y. Levy, J.N. Onuchic, Water and proteins: a love–hate relationship, Proc. Natl. Acad. Sci. 101 (2004) 3325–3326.

[3] L.C. Pardo, N. Veglio, F.J. Bermejo, J.L. Tamarit, G.J. Cuello, Experimental assessment of the extent of orientational short-range order in liquids, Phys. Rev. B 72 (2005) 014206.

[4] M. Jiménez-Ruiz, A. Criado, F.J. Bermejo, G.J. Cuello, F.R. Trouw, R. Fernández-Perea, H. Löwen, C. Cabrillo, H.E. Fischer, Purely dynamical signature of the orientational glass transition, Phys. Rev. Lett. 83 (1999) 2757–2760.

[5] P. Lloveras, A. Aznar, M. Barrio, P. Negrier, C. Popescu, A. Planes, L. Mañosa, E. Stern-Taulats, A. Avramenko, N.D. Mathur, X. Moya, J.L. Tamarit, Colossal barocaloric effects near room temperature in plastic crystals of neopentylglycol, Nat. Commun. 10 (2019) 1–7.

[6] A. Aznar, P. Lloveras, J.-Y. Kim, E. Stern-Taulats, M. Barrio, J.L. Tamarit, C.F. Sánchez-Valdés, J.L. Sánchez Llamazares, N.D. Mathur, X. Moya, Giant and reversible inverse barocaloric effects near room temperature in ferromagnetic mncogeb0. 03, Adv. Mater. 31 (2019) 1903577.

[7] M. Zachariah, M. Romanini, P. Tripathi, M. Barrio, J.L. Tamarit, R. Macovez, Self-diffusion, phase behavior, and li+ ion conduction in succinonitrile-based plastic cocrystals, J. Phys. Chem. C 119 (2015) 27298–27306.

[8] A. Criado, A. Muñoz, A molecular dynamics simulation of the plastic phase of hexachloroethane, Mol. Phys. 83 (1994) 815–833.

[9] A. Muñoz, A. Criado, A molecular dynamics interpretation of the inelastic neutron spectra in the plastic phase of hexachloroethane, Mol. Phys. 84 (1995) 1207–1225.

[10] P. Negrier, J.L. Tamarit, M. Barrio, D. Mondieig, Polymorphism in halogen-ethane derivatives: CCl_3 −−CCl_3 and ClF_2C−−CF_2Cl, Cryst. Growth Des. 13 (2013) 782–791.

[11] S. Seki, B. Momotani, Heats of transition of hexachloroethane, Bull. Chem. Soc. Japan 23 (1950) 30–31.

[12] P. Gerlach, D. Hohlwein, W. Prandl, F.W. Schulz, The plastic phase of hexachloroethane, C_2Cl_6: a neutron powder and single-crystal investigation, Acta Cryst. A37 (1981) 904–908.

[13] P. Gerlach, W. Prandl, J. Lefebvre, The plastic state of C_2Cl_6. a comparison of a monte carlo simulation of the molecular distribution with single crystal neutron data, Mol. Phys. 49 (1983) 991–999.

[14] P. Gerlach, W. Prandl, Short-range-order correlations in the orientationally disordered phase of hexachloroethane. i. Diffuse x-ray scattering, Acta Cryst. A44 (1988) 128–135.

[15] P. Gerlach, B. Dorner, W. Prandl, J. Lefebvre, Short-range-order correlations in the orientationally disordered phase of hexachloroethane. ii. Elastic and quasielastic neutron scattering, Acta Cryst. A44 (1988) 251–257.

[16] Y. Morino, M. Iwasaki, The estimation of the hindering potential barrier of hexachloroethane by electron diffraction investigation, J. Chem. Phys. 17 (1949) 216.

[17] D.A. Swick, I.L. Karle, J. Karle, The structure and internal motion of hexachloroethane, J. Chem. Phys. 22 (1952) 1242–1245.

[18] A. Henao, M. Rovira-Esteva, A. Vispa, J.L. Tamarit, E. Guàrdia, L.C. Pardo, Insights into the determination of molecular structure from diffraction data using a bayesian algorithm, J. Phys.: Condens. Matter 25 (2013) 454217.

[19] Y.L. Slovokhotov, A.S. Batsanov, J.A. Howard, Molecular van der waals symmetry affecting bulk properties of condensed phases: melting and boiling points, Struct. Chem. 18 (2007) 477–491.

[20] A. Henao, S. Pothoczki, M. Canales, E. Guàrdia, L.C. Pardo, Competing structures within the first shell of liquid C_2Cl_6: a molecular dynamics study, J. Mol. Liq. 190 (2014) 121–125.

[21] L.C. Pardo, A. Henao, A. Vispa, Characterizing ordering in liquids: an information theoretic approach, J. Non-Cryst. Solids 407 (2015) 220–227.

[22] K. Lindorff-Larsen, J. Ferkinghoff-Borg, Similarity measures for protein ensembles, PloS One 4 (2009) e4203.

[23] D.L. Beveridge, G. Barreiro, K.S. Byun, D.A. Case, T.E. Cheatham III, S.B. Dixit, E. Giudice, F. Lankas, R. Lavery, J.H. Maddocks, et al., Molecular dynamics simulations of the 136 unique tetranucleotide sequences of dna oligonucleotides. i. research design and results on d (cpg) steps, Biophys. J. 87 (2004) 3799–3813.

[24] J. Ballon, V. Comparat, J. Pouxe, The blade chamber: A solution for curved gaseous detectors, Nucl. Instrum. Methods Phys. Res. 217 (1983) 213–216.

[25] M. Evain, P. Deniard, A. Jouanneaux, R. Brec, Potential of the inel x-ray position-sensitive detector: a general study of the debye–scherrer setting, J. Appl. Cryst. 26 (1993) 563–569.

[26] B. Hess, C. Kutzner, D.V. der Spoel, E. Lindahl, Gromacs4: algorithms for highly efficient, load-balanced and scalable molecular simulation, J. Chem. Theory Comput. 4 (2008) 435–447.

[27] C. Oostenbrik, A. Villa, A.E. Mark, W.F.V. Gunsteren, A biomolecular force field based on the free enthalpy of hydration and solvation: the gromos force-field parameters sets 53a5 and 53a6, J. Comp. Chem. 25 (2004) 1656–1676.

[28] H. Goldstein, C.P. Poole, J.L. Safko, Classical Mechanics, third ed., Addison Wesley, San Francisco, 2002.

[29] A. Henao, S. Busch, E. Guàrdia, J.L. Tamarit, L.C. Pardo, The structure of liquid water beyond the first hydration shell, Phys. Chem. Chem. Phys. 18 (2016) 19420–19425.

[30] H.E. Fischer, G.J. Cuello, P. Palleau, D. Feltin, A.C. Barnes, Y.S. Badyal, J.M. Simonson, D4c: a very high precision diffractometer for disordered materials, Appl. Phys. A: Mater. Sci. Process. 74 (2002) S160.

[31] J.S. Pedersen, D. Posselt, K. Mortensen, Analytical treatment of the resolution function for small-angle scattering, J. Appl. Cryst. 23 (1990) 321–333.

[32] M. Rovira-Esteva, N. Murugan, L. Pardo, S. Busch, J.L. Tamarit, S. Pothoczki, G. Cuello, F.J. Bermejo, Interplay between intramolecular and intermolecular structures of 1, 1, 2, 2-tetrachloro-1, 2difluoroethane, Phys. Rev. B 84 (2011) 064202.

[33] D. Laage, Reinterpretation of the liquid water quasi-elastic neutron scattering spectra based on a nondiffusive jump reorientation mechanism, J. Phys. Chem. B 113 (2009) 2684–2687.

[34] A. Henao, J.M. Salazar-Rios, E. Guardia, L.C. Pardo, Structure and dynamics of water plastic crystals from computer simulations, J. Chem. Phys. 154 (2021) 104501.